Biogeosciences
Discussions

Open Access

EGU

Modelling spatial and temporal dynamics of GPP in the Sahel from earth observation based photosynthetic capacity and quantum efficiency

Torbern Tagesson[1], Jonas Ardö[2], Bernard Cappelaere[3], Laurent Kergoat[4], Abdulhakim M. Abdi[2], Stéphanie Horion[1], Rasmus Fensholt[1]

[1]Department of Geosciences and Natural Resource Management, University of Copenhagen, Øster Voldgade 10, DK-1350 Copenhagen, Denmark; E-Mails: torbern.tagesson@geo.ku.dk, stephanie.horion@geo.ku.dk, rf@geo.ku.dk

[2]Department of Physical Geography and Ecosystem Science, Lund University, Sölvegatan 12, SE- 223 62 Lund, Sweden, E-Mails: jonas.ardo@nateko.lu.se, hakim.abdi@gmail.com

[3]HydroSciences Montpellier, IRD, CNRS, Univ. Montpellier, Montpellier, France, E-Mail: bernard.cappelaere@um2.fr

[4]Geoscience Environnement Toulouse, (CNRS/UPS/IRD), 14 av E Belin, 31400 Toulouse, France, E-Mail: laurent.kergoat@get.obs-mip.fr

Correspondence to: Torbern Tagesson (torbern.tagesson@ign.ku.dk)

Abstract. It has been shown that vegetation growth in semi-arid regions is an important sink for human induced fossil fuel emissions of CO_2, which indicates the strong need for improved understanding, and spatially explicit estimates of CO_2 uptake (gross primary productivity (GPP)) in semi-arid ecosystems. This study has three aims: 1) to evaluate the MOD17A2H GPP (collection 6) product against eddy covariance (EC) based GPP for six sites across the Sahel. 2) To find evidence on the relationships between spatial and temporal variability in EC based photosynthetic capacity (F_{opt}) and quantum efficiency (α) and earth observation (EO) based vegetation indices 3) To study the applicability of EO up-scaled F_{opt} and α for GPP modelling purposes. MOD17A2H GPP (collection 6) underestimated GPP strongly, most likely because the maximum light use efficiency is set too low for semi-arid ecosystems in the MODIS algorithm. The intra-annual dynamics in F_{opt} was closely related to the shortwave infrared water stress index (SIWSI) closely coupled to equivalent water thickness, whereas α was closely related to the renormalized difference vegetation index (RDVI) affected by chlorophyll abundance. Spatial and inter-annual dynamics in F_{opt} and α were closely coupled to the normalized difference vegetation index (NDVI) and RDVI, respectively. Modelled GPP based on F_{opt} and α up-scaled using EO based indices reproduced in situ GPP well for all but a cropped site. The cropped site was strongly impacted by intensive anthropogenic land use. This study indicates the strong applicability of EO as a tool for parameterising spatially explicit estimates of photosynthetic capacity and efficiency; incorporating this into dynamic global vegetation models could improve global estimations of vegetation productivity, ecosystem processes and biochemical and hydrological cycles.

40   **1 Introduction**

41   Vegetation growth in semi-arid regions is an important sink for human induced fossil fuel emissions. Semi-arid regions

42   are even the main biome driving long-term trends and inter-annual variability in carbon dioxide (CO_2) uptake by

43   terrestrial ecosystems (Ahlström et al., 2015; Poulter et al., 2014). It is thus important to understand the long-term

44   variability of vegetation growth in semi-arid areas and their response to environmental conditions to better quantify and

45   forecast the effects of climate change.

46   The Sahel is a semi-arid transition zone between the dry Sahara desert in the North and the humid Sudanian savanna

47   in the south. The region has experienced numerous severe droughts during the last decades that resulted in region-wide

48   famines in 1972-1973 and 1984–1985 and localized food shortages across the region in 1990, 2002, 2004, 2011 and

49   2012 (Abdi et al., 2014; United Nations, 2013). Vegetation productivity is thereby an important ecosystem service for

50   the people living in the Sahel, but it is under high pressure. The region experiences a strong population growth,

51   increasing the demand on the ecosystem services due to cropland expansion, increased pasture stocking rates and

52   fuelwood extraction (Abdi et al., 2014). Continuous cropping is practised to meet the demand of the growing population

53   and has resulted in reduced soil fertility, which affects vegetation productivity negatively (Samaké et al., 2005; Chianu

54   et al., 2006).

55   At the same time as we have reports of declining vegetation productivity, we have contradicting reports of greening of

56   the Sahel based on remote sensing data (Dardel et al., 2014; Fensholt et al., 2013). The greening of the Sahel has mainly

57   been attributed to alleviated drought stress conditions due to increased precipitation since the mid-1990s (Hickler et al.,

58   2005). Climate is thus another important factor regulating vegetation productivity and semi-arid regions, such as the

59   Sahel, are particularly vulnerable to climate fluctuations due to their vulnerability to moisture conditions.

60   Estimation of gross primary productivity (GPP), i.e. uptake of atmospheric CO_2 by vegetation, is still a major

61   challenge within remote sensing of ecosystem services. GPP is a main driver of ecosystem services such as climate

62   regulation, carbon (C) sequestration, C storage, food production, or livestock grassland production. Within earth

63   observation (EO), spatial quantification of GPP generally involves light use efficiency (LUE), defined as the efficiency

64   to convert absorbed solar light into CO_2 uptake (Monteith, 1972, 1977). It has been shown that LUE varies in space and

65   time due to factors such as plant functional type, drought and temperature, nutrient levels and physiological limitations

66   of photosynthesis (Garbulsky et al., 2010; Paruelo et al., 2004; Kergoat et al., 2008). The LUE concept has been applied

67   using various methods, either by using a biome-specific LUE constant (Ruimy et al., 1994), or by modifying a

68   maximum LUE using meteorological variables (Running et al., 2004).

69   An example of an LUE based model is the standard GPP product from the Moderate Resolution Imaging

70   Spectroradiometer (MODIS) sensor (MOD17A2). Within the model, absorbed photosynthetically active radiation

71   (PAR) is estimated as a product of the fraction of PAR absorbed by the green vegetation (FPAR from MOD15A2)

72   multiplied with daily PAR from the meteorological data of the Global Modeling and Assimilation Office (GMAO). A

73   set of maximum LUE parameters specified for each biome are extracted from a Biome Properties Look-Up Table

74   (BPLUT). Then maximum LUE is modified depending on air temperature (T_{air}) and vapor pressure deficit (VPD) levels

75   (Running et al., 2004). Sjöström et al. (2013) evaluated the MOD17A2 product (collection 5.1) for Africa, and showed

76   that it was underestimating GPP for semi-arid savannas in the Sahel. Explanations for this underestimation were that the

77   assigned maximum LUE from the BPLUT is set too low and uncertainties in the FPAR (MOD15A2) product. Recently,

78   a new collection of MOD17A2 at 500 m spatial resolution was released (MOD17A2H; collection 6) with an updated

79   BPLUT, updated GMAO meteorological data, improved quality control and gap filling of the FPAR data from

80   MOD15A2 (Running and Zhao, 2015).

81   It has been shown that the LUE method does not perform well in arid conditions and at agricultural sites (Turner et

82   al., 2005). Additionally, the linearity assumed by the LUE model is usually not found as the response of GPP to

83   incoming light follows more of an asymptotic curve (Cannell and Thornley, 1998). Investigating other methods for

84   remotely determining GPP is thus of great importance, especially for semi-arid environments. Therefore, instead of

85   LUE we focus on the light response function of GPP at the canopy scale, and spatial and temporal variation of its two

86   main parameters: maximum GPP under light saturation (canopy-scale photosynthetic capacity; F_{opt}), and the initial

87   slope of the light response function (canopy-scale quantum efficiency; α) (Falge et al., 2001; Tagesson et al., 2015a).

88   Photosynthetic capacity is a measure of the maximum rate at which the canopy can fix CO_2 during photosynthesis

89   ($\mu mol\ CO_2\ m^{-2}\ s^{-1}$) whereas α is the amount of CO_2 fixed per incoming PAR ($\mu mol\ CO_2\ \mu mol\ PAR^{-1}$). Just to clarify the

90   difference in LUE and α in this study; LUE ($\mu mol\ CO_2\ \mu mol\ APAR^{-1}$) is the slope of a linear fit between CO_2 uptake

91   and absorbed PAR, whereas α ($\mu mol\ CO_2\ \mu mol\ PAR^{-1}$) is the initial slope of an asymptotic curve against incoming

92   PAR.

93   It has been proven that F_{opt} and α are closely related to chlorophyll abundance due to their coupling with the electron

94   transport rate (Ide et al., 2010). Additionally, in semi-arid ecosystems water availability is generally considered to be

95   the main limiting factor affecting intra-annual dynamics of vegetation growth (Fensholt et al., 2013; Hickler et al.,

96   2005; Tagesson et al., 2015b). Several remote sensing studies have established relationships between remotely sensed

97   vegetation indices and ecosystem properties such as chlorophyll abundance and equivalent water thickness (Yoder and

98   Pettigrew-Crosby, 1995; Fensholt and Sandholt, 2003). In this study we will analyse if EO vegetation indices can be

99   used for up-scaling F_{opt} and α and investigate if this could offer a promising way to map GPP in semi-arid areas. This

100   potential will be analysed by the use of detailed ground observations from six different measurement sites (eddy

101   covariance flux towers) across the Sahel.

102   The three aims of this study are:

103   1) To evaluate the recently released MOD17A2H GPP (collection 6) product and to investigate if it is better at

104   capturing GPP levels for the Sahel than collection 5.1. We hypothesise that MOD17A2H GPP (collection 6)

105   product will estimate GPP well for the six Sahelian measurement sites, because of the major changes done in

106   comparison to collection 5.1 (Running and Zhao, 2015).

107   2) To find evidence on the relationships between spatial and temporal variability in F_{opt} and α and remotely

108   sensed vegetation indices. We hypothesise that remotely sensed vegetation indices that are closely related to

109   chlorophyll abundance can be used for quantifying spatial and inter-annual dynamics in F_{opt} and α. Vegetation

110   indices closely related to equivalent water thickness are closely linked to intra-annual dynamics in F_{opt} and α

111   across the Sahel.

112   3) To evaluate the applicability of a GPP model based on the light response function using remotely sensed

113   vegetation indices and incoming PAR as input data.

2 Materials and Methods

2.1 Site description

The Sahel stretches from the Atlantic Ocean in the west to the Red Sea in the east. The northern border towards the Sahara and the southern border towards the humid Sudanian Savanna are defined by the 150 and 700 mm isohytes, respectively (Fig. 1) (Prince et al., 1995). Tree and shrub canopy cover is now generally low (< 5%) and dominated by species of *Balanites*, *Acacia, Boscia* and *Combretaceae* (Rietkerk et al., 1996). Annual grasses such as *Schoenefeldia gracilis*, *Dactyloctenium aegypticum*, *Aristida mutabilis*, and *Cenchrus biflorus* dominate the herbaceous layer, but perennial grasses such as *Andropogon gayanus*, *Cymbopogon schoenanthus* can also be found (Rietkerk et al., 1996; de Ridder et al., 1982). From the FLUXNET database (Baldocchi et al., 2001), we selected the six available measurement sites with eddy covariance based CO_2 flux data from the Sahel (Table 1; Fig. 1). The sites represent a variety of the ecosystems present in the region, from dry fallow bush savanna to seasonally inundated acacia forest. For a full description of the measurement sites, we refer to (Tagesson et al., 2016) and the references in Table 1.

<Table 1>

<Figure 1>

2.2 Data collection

2.2.1 Eddy covariance, hydrological and meteorological in situ data

Eddy covariance (EC), hydrological and meteorological data originating from the years between 2005 and 2013 were collected from the principal investigators of the measurement sites (Tagesson et al., 2016). The EC sensor set-up consisted of open-path CO_2/H_2O infrared gas analysers and 3-axis sonic anemometers. Data were collected at 20 Hz rate and statistics were calculated for 30-min periods. For a full description of sensor set up and post processing of the EC data, see references in Table 1. Final fluxes were filtered according quality flags provided by FLUXNET and outliers were filtered according Papale et al. (2006). We extracted the original net ecosystem exchange (NEE) data without any gap-filling or partitioning of NEE to GPP and ecosystem respiration. We also collected hydrological and meteorological data: air temperature (T_{air}; °C), rainfall (P; mm), relative air humidity (Rh; %), soil moisture at 0.1 m depth (SWC; % volumetric water content), incoming global radiation (R_g; W m^{-2}), incoming photosynthetically active radiation (PAR; μmol m^{-2} s^{-1}), VPD (hPa), peak dry weight biomass (g dry weight m^{-2}), C3/C4 species ratio, and soil conditions (nitrogen and C concentration; %). For a full description of the collected data and sensor set-up, see Tagesson et al. (2016).

2.2.2 Earth Observation data and gridded ancillary data

Remotely sensed composite products from the MODIS/Terra L4 from the Sahel were collected at Reverb ECHO (NASA, 2016). The collected products were GPP (MOD17A2H; collection 6) and the Nadir Bidirectional Reflectance Distribution Function (BRDF) adjusted reflectance (NBAR) (8-day composites; MCD43A4; collection 5.1) at 500*500 m^2 spatial resolution, and the normalized difference vegetation index (NDVI), and the enhanced vegetation index (EVI) (16-day composites; MOD13Q1; collection 6) at 250*250 m^2 spatial resolution. The NBAR product was preferred over the reflectance product (MOD09A1), in order to avoid variability caused by varying sun and sensor viewing geometry (Huber et al., 2014; Tagesson et al., 2015c). We extracted the median of the 3x3 pixels centred at the location of the EC towers. The time series of the remotely sensed products were filtered according the MODIS quality control data;

153 MOD17A2H is a gap-filled and filtered product, QC data from MCD43A2 were used for the filtering of MCD43A4;

154 and bit 2-5 (highest –decreasing quality) was used for MOD13Q1. Finally, data were gap-filled to daily values using

155 linear interpolation.

156 For a GPP model to be applicable on a larger spatial scale, a gridded data set of incoming PAR is needed. We

157 downloaded ERA Interim reanalysis PAR at the ground surface (W m^{-2}) with a spatial resolution of 0.25°×0.25°

158 accumulated for each 3-hour period 2000-2015 from the European Centre for Medium-Range Weather Forecasts

159 (ECMWF) (Dee et al., 2011; ECMWF, 2016).

160

161 **2.3 Data handling**

162 **2.3.1 Intra-annual dynamics in photosynthetic capacity and quantum efficiency**

163 Both linear and hyperbolic equations have been used for investigating the response of GPP to incoming light (Wall and

164 Kanemasu, 1990; Campbell et al., 2001). However, they do not represent the lower part of the light response function

165 particularly well, and we thereby instead choose to use the asymptotic Mitscherlich light-response function (Inoue et al.,

166 2008; Falge et al., 2001). The Mitscherlich light-response function was fitted between daytime NEE and incoming

167 PAR:

168 $$NEE = -(F_{opt}) \times (1 - e^{\left(\frac{-\alpha \times PAR}{F_{opt}}\right)}) + R_d \qquad (1)$$

169 where F_{opt} is the CO_2 uptake at light saturation (photosynthetic capacity; μmol CO_2 m^{-2} s^{-1}), R_d is dark respiration

170 (μmol CO_2 m^{-2} s^{-1}), and α is the initial slope of the light response curve (quantum efficiency; μmol CO_2 μmol PAR^{-1})

171 (Falge et al., 2001). By subtracting R_d from Eq. 1, the function is forced through zero and GPP is thereby estimated. We

172 fitted Eq. 1 using 7-day moving windows with 1 day time steps and generating daily values of F_{opt} and α. To assure high

173 quality of the fitted parameters, parameters were excluded from the analysis when the fitting was insignificant (p-

174 value<0.05), and when they were out of range (F_{opt} and α >peak value of the rainy season times 1.2). Additionally,

175 outliers were filtered following the method by Papale et al. (2006) using 30-day moving windows with 1 day time steps.

176

177 **2.3.2 Vegetation indices**

178 We analysed the relationship between F_{opt}, α and some commonly applied vegetation indices:

179 The maximum absorption in the red wavelengths generally occurs at 682 nm as this is the peak absorption for

180 chlorophyll a and b (Thenkabail et al., 2000), which makes vegetation indices that include the red band sensitive to

181 chlorophyll abundance. By far the most common vegetation index is the NDVI (Rouse et al., 1974):

182 $$NDVI = \frac{(\rho_{NIR} - \rho_{red})}{(\rho_{NIR} + \rho_{red})} \qquad (2)$$

183 where ρ_{NIR} is the reflectance factor in the near infrared (NIR) band (band 2) and ρ_{red} is the reflectance factor in the red

184 band (band 1). The NIR radiance is scattered by the air-water interfaces between the cells whereas red radiance is

185 absorbed by chlorophyll and its accessory pigments (Gates et al., 1965). Normalization is done to reduce effects of

186 atmospheric errors, solar zenith angles, and sensor viewing geometry, as well as increasing the vegetation signal (Qi et

187 al., 1994; Inoue et al., 2008).

188   A well-known issue with the NDVI is that it saturates at high biomass because the absorption of red light at ~670 nm

189   peaks at higher biomass loads whereas NIR reflectance continues to increase due to multiple scattering effects

190   (Mutanga and Skidmore, 2004; Jin and Eklundh, 2014). By reducing atmospheric and soil background influences, EVI

191   increases the signal from the vegetation and maintain sensitivity in high biomass regions (Huete et al., 2002).

192   $$EVI = G \frac{(\rho_{NIR} - \rho_{red})}{(\rho_{NIR} + C_1 \rho_{red} - C_2 \rho_{blue} + L)} \qquad (3)$$

193   where ρ_{blue} is the reflectance factor in the blue band (band 3). The coefficients C_1=6 and C_2=7.5 correct for atmospheric

194   influences, while L=1 adjust for the canopy background. The factor G=2.5 is the gain factor.

195   Another attempt to overcome the issue of NDVI saturation was proposed by Roujean and Breon (1995), which

196   combines the advantages of the DVI (NIR-red) and the NDVI for low and high vegetation cover, respectively:

197   $$RDVI = \frac{(\rho_{NIR} - \rho_{red})}{\sqrt{(\rho_{NIR} + \rho_{red})}} \qquad (4)$$

198   As a non-linear index, RDVI is not only less sensitive to variations in the geometrical and optical properties of

199   unknown foliage but also less affected by the solar and viewing geometry (Broge and Leblanc, 2001).

200   The NIR and SWIR bands are affected by the same ground properties, except that SWIR bands are also strongly

201   sensitive to equivalent water thickness. Fensholt and Sandholt (2003) proposed a vegetation index, the shortwave

202   infrared water stress index (SIWSI), using NIR and SWIR bands to estimate drought stress for vegetation in semi-arid

203   environments:

204   $$SIWSI_{12} = \frac{(\rho_{NIR} - \rho_{SWIR12})}{(\rho_{NIR} + \rho_{SWIR12})} \qquad (5)$$

205   $$SIWSI_{16} = \frac{(\rho_{NIR} - \rho_{SWIR16})}{(\rho_{NIR} + \rho_{SWIR16})} \qquad (6)$$

206   where ρ_{swir12} is NBAR band 5 (1230-1250 nm) and ρ_{swir16} is NBAR band 6 (1628-1652 nm). As the vegetation water

207   content increases, the reflectance in the SWIR decreases indicating that low and high SIWSI values point to sufficient

208   water conditions and drought stress, respectively.

209

210   **2.3.3 Incoming PAR across the Sahel**

211   Incoming PAR at the ground surface from ERA Interim followed the pattern of PAR measured at the six sites in situ

212   closely, but it was systematically underestimated (Fig. 2). An ordinary least square linear regression was thereby fitted

213   between ERA Interim PAR and PAR measured in situ ($PAR_{in\ situ}$=3.09* $PAR_{ERA\ interim}$ +23.07; coefficient of

214   determination (R^2)=0.93; n=37976). The regression line was used for converting ERA Interim PAR to the same level as

215   in situ measured PAR.

216   <Figure 2>

217

218   **2.4 Data analysis**

219   **2.4.1 Coupling temporal and spatial dynamics in photosynthetic capacity and quantum efficiency with**

220   **explanatory variables**

221   In a first step, the coupling between intra-annual dynamics in F_{opt} and α and the vegetation indices for the different

222   measurement sites were studied using Pearson correlation analysis. Relationships between intra-annual dynamics in F_{opt}

223   and α and the vegetation indices for all sites combined were also analysed. In order to avoid influence of the spatial and

224   inter-annual variability, time series of ratios of F_{opt} and α (F_{opt_frac} and α_{frac}) against the annual peak values (F_{opt_peak} and

225   α_{peak}; see below for calculation of annual peak values) were estimated for all sites:

226     $$F_{opt\_frac} = \frac{F_{opt}}{F_{opt\_peak}} \qquad\qquad (7)$$

227     $$\alpha_{frac} = \frac{\alpha}{\alpha_{peak}} \qquad\qquad (8)$$

228   The same standardisation procedure was used for all vegetation indices (VI_{frac}):

229     $$VI_{frac} = \frac{VI}{VI_{peak}} \qquad\qquad (9)$$

230   where VI_{peak} is the annual peak values of the vegetation indices (14 days running mean with highest annual value). Such

231   a standardisation gives fractions of how F_{opt}, α and VI varies over the season in relationship to the annual peak value,

232   and it removes the spatial and inter-annual variation, and mainly intra-annual dynamics remains. The coupling between

233   α_{frac} and F_{opt_frac} and the different VI_{frac} were examined using Pearson correlation analysis for all sites. The robustness of

234   the correlation coefficients was estimated by using a bootstrap simulation with 200 iterations in the correlation analysis

235   (Richter et al., 2012).

236   In order to investigate spatial and inter-annual variability in F_{opt} and α for the measurement sites, gaps needed to be

237   filled. Regression trees were used to fill gaps in the daily estimates of F_{opt} and α. One hundred tree sizes were chosen

238   based on 100 cross validation runs, and these trees were then used for estimating the F_{opt} and α (De'ath and Fabricius,

239   2000). We used SWC, VPD, T_{air}, PAR, and the vegetation index with strongest correlation with intra-annual dynamics

240   as explanatory variables in the analysis. In the analysis for all sites, the same standardisation procedure as done for F_{opt},

241   α, and the vegetation indices was done for the hydrological and meteorological variables. The 100 F_{opt} and α output

242   subsets from the regression trees were averaged and used for filling the gaps in F_{opt} and α.

243   To investigate spatial and inter-annual variability in F_{opt} and α across the measurement sites of the Sahel, annual peak

244   values of F_{opt} and α (F_{opt_peak} and α_{peak}; 14 days running mean with highest annual value) were correlated with the annual

245   sum of P, yearly means of T_{air}, SWC, RH, VPD, R_g, annual peak values of biomass, soil nitrogen and C concentrations,

246   C3/C4 ratio, and VI_{peak} using Pearson linear correlations. Again, we used a bootstrap simulation methodology with 200

247   iterations in order to estimate the robustness of the correlations.

248

249   2.4.2 The GPP model

250   Based on Eq. 1 and the outcome of the statistical analysis previously described under subsection 2.4.1 (for results see

251   subsect. 3.2), a model for estimating GPP across the Sahel was created:

252     $$GPP = -F_{opt} \times \left(1 - e^{\left(\frac{-\alpha \times PAR}{F_{opt}}\right)}\right) \qquad\qquad (10)$$

253 The model is applicable for each point in space and time. Firstly, F_{opt_peak} and α_{peak} were estimated spatially and inter-

254 annually using linear regression functions fitted against the vegetation indices with the strongest relationships to spatial

255 and inter-annual variability in F_{opt_peak} and α_{peak}:

256 $$F_{opt\_peak} = k_{Fopt} \times NDVI_{peak} + m_{Fopt} \tag{11}$$

257 $$\alpha_{peak} = k_\alpha \times RDVI_{peak} + m_\alpha \tag{12}$$

258 where k_{Fopt} and k_α are the slopes of the lines and m_{Fopt} and m_α are the intercepts. Secondly, to estimate the F_{opt_frac} and

259 α_{frac} for each day of the year, linear regression functions were established for F_{opt_frac} and α_{frac} with the vegetation index

260 with the strongest relationships to intra-annual variability of F_{opt_frac} and α_{frac} for all sites, as follows:

261 $$F_{opt\_frac} = l_{Fopt} \times RDVI_{frac} + n_{Fopt} \tag{13}$$

262 $$\alpha_{frac} = l_\alpha \times RDVI_{frac} + n_\alpha \tag{14}$$

263 where l_{Fopt} and l_α are the slopes of the lines and n_{Fopt} and n_α are the intercepts. Eq. 11-14 provide the relationships to

264 estimate F_{opt} and α for any day of the year and for any point in space across the Sahel:

265 $$F_{opt} = F_{opt\_peak} \times F_{opt\_frac} = \left(k_{Fopt} \times NDVI_{max} + m_{Fopt}\right)\left(l_{Fopt} \times RDVI_{frac} + n_{Fopt}\right) \tag{15}$$

266 $$\alpha = \alpha_{peak} \times \alpha_{frac} = \left(k_\alpha \times RDVI_{max} + m_\alpha\right)\left(l_\alpha \times RDVI_{frac} + n_\alpha\right) \tag{16}$$

267 Eq. 15 and 16 can be put into Eq. 10 and GPP is thereafter estimated as:

268 $$GPP = -\left(F_{opt\_peak} \times F_{opt\_frac}\right) \times \left(1 - e^{\left(\frac{-\left(\alpha_{peak} \times \alpha_{frac}\right) \times PAR}{F_{opt\_peak} \times F_{opt\_frac}}\right)}\right) \tag{17}$$

269 generating a final model as:

270 $$GPP = -\left(\left(k_{Fopt} \times NDVI_{max} + m_{Fopt}\right)\left(l_{Fopt} \times RDVI_{frac} + n_{Fopt}\right)\right)$$
$$\times \left(1 - e^{\left(\frac{-\left(k_\alpha \times NDVI_{max} + m_\alpha\right)\left(l_\alpha \times RDVI_{frac} + n_\alpha\right) \times PAR}{\left(k_{Fopt} \times NDVI_{max} + m_{Fopt}\right)\left(l_{Fopt} \times RDVI_{frac} + n_{Fopt}\right)}\right)}\right) \tag{18}$$

271

272 **2.4.3 Parameterisation and evaluation of modelled GPP and evaluation of the MODIS GPP product**

273 In order to estimate the robustness of the GPP model and its parameters, we used a bootstrap simulation methodology

274 when fitting the empirical relationships. We used 200 iterations and different measurement sites were used in the

275 different runs when fitting the empirical relationships (Richter et al., 2012). The runs generated 200 sets of slopes,

276 intercepts, and R^2, from which the medians and the standard deviations were estimated. Possible errors (e.g. random

277 sampling errors, aerosols, electrical sensor noise, filtering and gap-filling errors, clouds, and satellite sensor

278 degradation) can be present in both the predictor and the response variables. Hence, we selected reduced major axis

279 linear regressions to account for errors in both predictor and response variables when fitting the regression functions.

280 The regression models were validated against the left-out subsamples within the bootstrap simulation methodology by

281 calculating the root-mean-square-error (RMSE), and by fitting an ordinary least squares linear regression between

282 modelled and in situ variables.

283 Similarly, the MODIS GPP product (MOD17A2H, collection 6) was evaluated against in situ GPP by calculating

284 RMSE, and by fitting an ordinary least squares linear regression.

285

286   **3 Results**

287   **3.1 Evaluation of the MODIS GPP product**

288   There was a strong linear relationship between the MODIS GPP product (MOD17A2H; collection 6) and the in situ

289   GPP (slope 0.17; intercept 0.11 g C m^{-2} d^{-1}; R^2 0.69; n=598). However, MOD17A2H strongly underestimated in situ

290   GPP (Fig. 3) resulting in high RMSE (2.69 g C m^{-2} d^{-1}).

291   <Figure 3>

292

293   **3.2 Intra-annual dynamics in photosynthetic capacity and quantum efficiency**

294   Intra-annual dynamics in F_{opt} and α differed in amplitude, but were otherwise similar across the measurement sites in

295   the Sahel (Fig. 4). There is no green ground vegetation during the dry season, and the low photosynthetic activity is due

296   to few evergreen trees. This results in low values for both F_{opt} and α during the dry season. The vegetation responded

297   strongly to rainfall, and both F_{opt} and α increased during the early phase of the rainy season. Generally, F_{opt} peaked

298   slightly earlier than α (average± 1 standard deviation: 7±10 days) (Fig. 4).

299   <Figure 4>

300   All vegetation indices described intra-annual dynamics in F_{opt} well for all sites (Table 2). $SIWSI_{12}$ had the highest

301   correlation for all sites except Wankama Millet, where it was RDVI. When all sites were combined, all indices

302   described seasonality in F_{opt} well, but RDVI had the strongest correlation (Table 2).

303   The intra-annual dynamics in α were also closely coupled to intra-annual dynamics in the vegetation indices for all

304   sites (Table 2). For α, RDVI was the strongest index describing intra-annual dynamics, except for Wankama Fallow

305   where it was EVI. When all sites were combined all indices described intra-annual dynamics in α well, but RDVI was

306   still the index with the strongest relationship (Table 2).

307   <Table 2>

308   The regression trees used for gap-filling explained the intra-annual dynamics in F_{opt} and α well for all sites (Table 3).

309   The main explanatory variables coupled to intra-annual dynamics in F_{opt} for all sites across the Sahel were in the order

310   of RDVI, SWC, VPD, T_{air}, and PAR; and for α they were RDVI, SWC, VPD and T_{air}. For all sites across Sahel,

311   incorporating hydrological and meteorological variables increased the ability to determine intra-annual dynamics in F_{opt}

312   and α compared to the ordinary least squares linear regressions against the RDVI (Table 2, data given as *r;* Table 3).

313   The incorporation of these variables increased the R^2 from 0.81 to 0.87 and from 0.74 to 0.84, for F_{opt} and α

314   respectively.

315   <Table 3>

316

317   **3.3 Spatial and inter-annual dynamics in photosynthetic capacity and quantum efficiency**

318   Large spatial and inter-annual variability in F_{opt_peak} and α_{peak} were found across the six measurement sites in the Sahel

319   (Table 4). The average two week running mean peak values of F_{opt} and α for all sites were 26.4 μmol CO_2 m^{-2} s^{-1} and

320   0.040 μmol CO_2 μmol PAR^{-1}, respectively. However, the ranges were large; F_{opt_peak} ranged between 10.1 μmol CO_2 m^{-2} s^{-1}

321   ^{2} s^{-1} (Wankama Millet 2005) and 50.0 μmol CO_2 m^{-2} s^{-1} (Dahra 2010), and α_{peak} ranged between 0.020

322   μmol CO_2 μmol PAR^{-1} (Demokeya 2007) and 0.064 μmol CO_2 μmol PAR^{-1} (Dahra 2010) (Table 4). All vegetation

323   indices determined spatial and inter-annual dynamics in F_{opt_peak} and α_{peak} well (Table 5). $NDVI_{peak}$ was most closely

324   coupled with F_{opt_peak} whereas $RDVI_{peak}$ was closest coupled with α_{peak} (Fig. 5). F_{opt_peak} also correlated well with peak

325   dry weight biomass, C content in the soil, and RH, whereas α_{peak} also correlated well with peak dry weight biomass, and

326   C content in the soil (Table 5).

327   <Table 4>

328   <Table 5>

329   <Figure 5>

330

331   **3.4 Evaluation of the GPP model**

332   Modelled GPP was similar to in situ GPP on average, and there was a strong linear relationship between modelled GPP

333   and in situ GPP for all sites (Fig. 6; Table 6). However, when separating the evaluation between measurement sites, it

334   can be seen that the model reproduced some sites better than others (Figure 7; Table 6). Wankama Millet is generally

335   overestimated whereas the model works on average well for Demokeya but underestimates high values (Fig. 7; Table

336   6). Variability of in situ GPP at the other sites is well reproduced by the model (Fig. 7; Table 6). The final parameters

337   of the GPP model (Eq. 18) are given in Table 7.

338   <Figure 6>

339   <Figure 7>

340   < Table 6>

341   < Table 7>

342

343   **4 Discussion**

344   Vegetation productivity of semi-arid savanna ecosystems is primarily driven by intra-annual rainfall distribution

345   (Eamus et al., 2013; Brümmer et al., 2008; Moncrieff et al., 1997), and in the Sahel soil moisture conditions at the early

346   rainy season are especially important (Rockström and de Rouw, 1997; Tagesson et al., 2016; Mbow et al., 2013). We

347   thereby hypothesised that vegetation indices closely related to equivalent water thickness (SIWSI) would be strongly

348   linked to intra-annual dynamics in F_{opt} and α. Our hypothesis was not rejected for F_{opt}, since this was also the case for

349   all sites except for Wankama Millet (Table 2). The Wankama millet is a cropped agricultural site whereas all other sites

350   are savanna ecosystems. However, our hypothesis was rejected for α, since it was more closely related to vegetation

351   indices related to chlorophyll abundance (RDVI and EVI). Leaf area index increases over the growing season and it is

352   closely related to the vegetation indices coupled with chlorophyll abundance (Tagesson et al., 2009). This increases the

353   canopy level quantum efficiency (α) which explains the close relationship of α to RDVI. However, F_{opt} peaked earlier in

354   the rainy season than α (Fig. 4). Vegetation during this phase is vulnerable to drought conditions explaining the close

355   relationship of F_{opt} to SIWSI. F_{opt} can only increase up to a certain level due to other constraining factors (nutrient,

356   water and meteorological conditions) which could explain its closer relationship with $SIWSI_{12}$ than with RDVI.

357   We hypothesised that remotely sensed vegetation indices closely related to chlorophyll abundance can be used for

358   quantifying spatial and inter-annual dynamics in F_{opt} and α. Indeed, NDVI, EVI, and RDVI all had close correlations

359   with the spatial and inter-annual dynamics in F_{opt} and α (Table 5). It was surprising that $NDVI_{peak}$ had the strongest

360   correlation with spatial and inter-annual variability for F_{opt} (Table 5). Both EVI and RDVI should be less sensitive to

361   saturation effects than NDVI (Huete et al., 2002; Roujean and Breon, 1995), and based on this we assumed that peak

362   values of these indices should have stronger relationships to peak values of F_{opt} and α. However, vegetation indices with

363   a high sensitivity to changes in green biomass at high biomass loads, gets less sensitive to green biomass changes at low

364   biomass loads (Huete et al., 2002). Peak leaf area index for ecosystems across the Sahel is approximately 2, whereas the

365   saturation issue of NDVI generally starts at an leaf area index of about 2-5 (Haboudane et al., 2004). Additionally,

366   atmospheric scattering is much higher in the shorter wavelengths making EO-based vegetation indices including blue-

367   band information very sensitive to the atmospheric correction (Fensholt et al., 2006b), possibly explaining the lower

368   correlation for EVI.

369   Our model substantially overestimates GPP for Wankama Millet (Fig. 7f). As a crop field, this site differs in particular

370   from the other studied sites by its species composition, ecosystem structure, as well as land and vegetation management.

371   Crop fields in southwestern Niger are generally characterized by a rather low productivity resulting from decreased

372   fertility and soil loss caused by intensive land use (Cappelaere et al., 2009). These specifics of the Wankama Millet site

373   may cause the model parameterised with observations from the other study sites to overestimate GPP at this site. The

374   model parameterised using observation from the other measurement sites without this strong anthropogenic influence

375   thus overestimates GPP. Similar results were found by Boulain et al. (2009) when applying an up-scaling model using

376   leaf area index for Wankama Millet and Wankama Fallow. It worked well for Wankama fallow whereas it was less

377   conclusive for Wankama Millet. The main explanation was low leaf area index in millet fields because of a low density

378   of millet stands due to agricultural practice. There is extensive savanna clearing for food production in the Sahel

379   (Leblanc et al., 2008; Boulain et al., 2009; Cappelaere et al., 2009). To further understand the impacts of this land cover

380   change on vegetation productivity and land atmosphere exchange processes, it is of urgent need for more study sites

381   covering cropped areas in this region.

382   In Demokeya, GPP is slightly underestimated for the year 2008 (Fig. 7c) because modelled F_{opt} (the thick black line in

383   Fig. 5) is much lower than the actual measured value in 2008. An improvement of the model could be to incorporate

384   some parameters that constrain or enhance F_{opt} depending on environmental stress. Indeed, the regression tree analysis

385   indicated that incorporating climatic and hydrological variables increased the ability to predict both F_{opt} and α. On the

386   other hand, for spatial upscaling purposes, it has been shown that including modelled climatic constraints on LUE

387   decreases the ability to predict vegetation productivity due to the incorporated uncertainty in these modelled

388   meteorological variables (Fensholt et al., 2006a; Ma et al., 2014). For spatial upscaling to regional scales it is therefore

389   better to simply use relationships to EO data. This is particularly the case for the Sahel, one of the largest dryland areas

390   in the world that is characterised by few sites of meteorological observations.

391   Although MOD17A2 GPP has previously been shown to capture GPP relatively well in several different ecosystems

392   (Turner et al., 2006; Turner et al., 2005; Heinsch et al., 2006; Sims et al., 2006; Kanniah et al., 2009), it has been shown

393   to be underestimated for others (Coops et al., 2007; Gebremichael and Barros, 2006; Sjöström et al., 2013). GPP of

394   Sahelian drylands have not been well captured by MOD17A2 (Sjöström et al., 2013; Fensholt et al., 2006a), and as we

395   have shown, this underestimation persists in the latest MOD17A2H GPP (collection 6) product. The main reason for

396   this major underestimation is that maximum LUE is set to 0.84 g C MJ^{-1} (open shrubland; Demokeya) and 0.86 g C MJ^{-}

397   ^{1} (grassland; Agofou, Dahra, Kelma; Wankama Millet and Wankama Fallow) in the BPLUT, i.e. much lower than

398   maximum LUE measured at the Sahelian measurement sites of this study (average: 2.47 g C MJ^{-1}; range: 1.58-3.50 g C

399   MJ^{-1}) (Sjöström et al., 2013; Tagesson et al., 2015a), a global estimate of ~1.5 g C MJ^{-1} (Garbulsky et al., 2010), and a

400   savanna site in Australia (1.26 g C MJ^{-1}) (Kanniah et al., 2009).

401   Several state of the art dynamic global vegetation models have been used for decades to quantify GPP at different

402   spatial and temporal scales (Dickinson, 1983; Sellers et al., 1997). These models are generally based on the

403 photosynthesis model by Farquhar et al. (1980), a model particularly sensitive to uncertainty in photosynthetic capacity

404 (Zhang et al., 2014). This and several previous studies have shown that both photosynthetic capacity and efficiency

405 (both α and LUE) can considerably vary seasonally and spatially, both within and between vegetation types (Eamus et

406 al., 2013; Garbulsky et al., 2010; Ma et al., 2014; Tagesson et al., 2015a). This variability is difficult to estimate using

407 broad values based on land cover classes, yet most models apply a constant value which can cause substantial

408 inaccuracies in the estimates of seasonal and spatial variability in GPP. This is particularly a problem in savannas that

409 comprises of several plant functional types (C3 and C4 species, and a large variability in tree/herbaceous vegetation

410 fractions) (Scholes and Archer, 1997). This study indicates the strong applicability of EO as a tool for parameterising

411 spatially explicit estimates of plant physiological variables, which could improve our ability to simulate GPP. Spatially

412 explicit estimates of GPP at a high temporal and spatial resolution are essential for current global change studies and

413 would be advantageous in the analysis of changes in GPP, its relationship to climatic change and anthropogenic forcing,

414 and estimations of ecosystem processes and biochemical and hydrological cycles.

415

423

424 **References**

425 Abdi, A., Seaquist, J., Tenenbaum, D., Eklundh, L., and Ardö, J.: The supply and demand of net

426 primary production in the Sahel, Environ. Res. Lett., 9, 094003, doi:10.1088/1748-9326/9/9/094003,

427 2014.

428 Ahlström, A., Raupach, M. R., Schurgers, G., Smith, B., Arneth, A., Jung, M., Reichstein, M.,

429 Canadell, J. G., Friedlingstein, P., Jain, A. K., Kato, E., Poulter, B., Sitch, S., Stocker, B. D., Viovy,

430 N., Wang, Y. P., Wiltshire, A., Zaehle, S., and Zeng, N.: The dominant role of semi-arid ecosystems

431 in the trend and variability of the land CO_2 sink, Science, 348, 895-899, 10.1126/science.aaa1668,

432 2015.

433 Baldocchi, D., Falge, E., Gu, L., Olson, R., Hollinger, D., Running, S., Anthoni, P., Bernhofer, C.,

434 Davis, K., Evans, R., Fuentes, J., Goldstein, A., Katul, G., Law, B., Lee, X., Malhi, Y., Meyers, T.,

435 Munger, W., Oechel, W., Paw, K. T., Pilegaard, K., Schmid, H. P., Valentini, R., Verma, S., Vesala,

436 T., Wilson, K., and Wofsy, S.: FLUXNET: A New Tool to Study the Temporal and Spatial

437 Variability of Ecosystem–Scale Carbon Dioxide, Water Vapor, and Energy Flux Densities, Bull.

438 Am. Meteorol. Soc., 82, 2415-2434, 10.1175/1520-0477(2001)082<2415:fantts>2.3.co;2, 2001.

439 Boulain, N., Cappelaere, B., Ramier, D., Issoufou, H. B. A., Halilou, O., Seghieri, J., Guillemin, F.,

440 Oï, M., Gignoux, J., and Timouk, F.: Towards an understanding of coupled physical and biological

441 processes in the cultivated Sahel – 2. Vegetation and carbon dynamics, J. Hydrol., 375, 190-203,

442 10.1016/j.jhydrol.2008.11.045, 2009.

443 Broge, N. H., and Leblanc, E.: Comparing prediction power and stability of broadband and

444 hyperspectral vegetation indices for estimation of green leaf area index and canopy chlorophyll

Biogeosciences

Discussions

Open Access

EGU

445   density, Remote Sens. Environ., 76, 156-172, http://dx.doi.org/10.1016/S0034-4257(00)00197-8,
446   2001.
447   Brümmer, C., Falk, U., Papen, H., Szarzynski, J., Wassmann, R., and Brüggemann, N.: Diurnal,
448   seasonal, and interannual variation in carbon dioxide and energy exchange in shrub savanna in
449   Burkina Faso (West Africa), J. Geophys. Res., 113, G02030, 10.1029/2007jg000583, 2008.
450   Campbell, C. S., Heilman, J. L., McInnes, K. J., Wilson, L. T., Medley, J. C., Wu, G., and Cobos, D.
451   R.: Seasonal variation in radiation use efficiency of irrigated rice, Agric. For. Meteorol., 110, 45-54,
452   http://dx.doi.org/10.1016/S0168-1923(01)00277-5, 2001.
453   Cannell, M., and Thornley, J.: Temperature and CO_2 Responses of Leaf and Canopy Photosynthesis:
454   a Clarification using the Non-rectangular Hyperbola Model of Photosynthesis, Ann. Bot., 82, 883-
455   892, 1998.
456   Cappelaere, B., Descroix, L., Lebel, T., Boulain, N., Ramier, D., Laurent, J. P., Favreau, G.,
457   Boubkraoui, S., Boucher, M., Bouzou Moussa, I., Chaffard, V., Hiernaux, P., Issoufou, H. B. A., Le
458   Breton, E., Mamadou, I., Nazoumou, Y., Oi, M., Ottlé, C., and Quantin, G.: The AMMA-CATCH
459   experiment in the cultivated Sahelian area of south-west Niger – Investigating water cycle response
460   to a fluctuating climate and changing environment, J. Hydrol., 375, 34-51,
461   10.1016/j.jhydrol.2009.06.021, 2009.
462   Chianu, J. N., Tsujii, H., and Awange, J.: Environmental impact of agricultural production practices
463   in the savannas of northern Nigeria J. Food Agric. Environ., 4, 255-260, 2006.
464   Coops, N. C., Black, T. A., Jassal, R. S., Trofymow, J. A., and Morgenstern, K.: Comparison of
465   MODIS, eddy covariance determined and physiologically modelled gross primary production (GPP)
466   in a Douglas-fir forest stand, Remote Sens. Environ., 107, 385-401,
467   http://dx.doi.org/10.1016/j.rse.2006.09.010, 2007.
468   Dardel, C., Kergoat, L., Hiernaux, P., Mougin, E., Grippa, M., and Tucker, C. J.: Re-greening Sahel:
469   30 years of remote sensing data and field observations (Mali, Niger), Remote Sens. Environ., 140,
470   350-364, http://dx.doi.org/10.1016/j.rse.2013.09.011, 2014.
471   De'ath, G., and Fabricius, K. E.: Classification and regression trees: A powerful yet simple
472   technique for ecological data analysis, Ecology, 81, 3178-3192, 10.2307/177409, 2000.
473   de Ridder, N., Stroosnijder, L., and Cisse, A. M.: Productivity of Sahelian rangelands : a study of
474   the soils, the vegetations and the exploitation of that natural resource, PPS course book. Primary
475   Production in the Sahel, Agricultural University, Wageningen, 1982.
476   Dee, D. P., Uppala, S. M., Simmons, A. J., Berrisford, P., Poli, P., Kobayashi, S., Andrae, U.,
477   Balmaseda, M. A., Balsamo, G., Bauer, P., Bechtold, P., Beljaars, A. C. M., van de Berg, L., Bidlot,
478   J., Bormann, N., Delsol, C., Dragani, R., Fuentes, M., Geer, A. J., Haimberger, L., Healy, S. B.,
479   Hersbach, H., Hólm, E. V., Isaksen, L., Kållberg, P., Köhler, M., Matricardi, M., McNally, A. P.,
480   Monge-Sanz, B. M., Morcrette, J. J., Park, B. K., Peubey, C., de Rosnay, P., Tavolato, C., Thépaut,
481   J. N., and Vitart, F.: The ERA-Interim reanalysis: configuration and performance of the data
482   assimilation system, Q. J. Roy. Meteor. Soc., 137, 553-597, 10.1002/qj.828, 2011.
483   Dickinson, R. E.: Land Surface Processes and Climate—Surface Albedos and Energy Balance, in:
484   Advances in Geophysics, edited by: Barry, S., Elsevier, 305-353, 1983.
485   Eamus, D., Cleverly, J., Boulain, N., Grant, N., Faux, R., and Villalobos-Vega, R.: Carbon and
486   water fluxes in an arid-zone Acacia savanna woodland: An analyses of seasonal patterns and
487   responses to rainfall events, Agric. For. Meteorol., 182–183, 225-238,
488   http://dx.doi.org/10.1016/j.agrformet.2013.04.020, 2013.
489   ECMWF: ERA Interim Daily: http://apps.ecmwf.int/datasets/data/interim-full-daily/levtype=sfc/,
490   access: 04-04-2016, 2016.
491   Falge, E., Baldocchi, D., Olson, R., Anthoni, P., Aubinet, M., Bernhofer, C., Burba, G., Ceulemans,
492   R., Clement, R., Dolman, H., Granier, A., Gross, P., Grunwald, T., Hollinger, D., Jensen, N. O.,

Biogeosciences

Discussions

Open Access

EGU

493 Katul, G., Keronen, P., Kowalski, A., Lai, C. T., Law, B. E., Meyers, T., Moncrieff, J. B., Moors, E.,
494 Munger, J. W., Pilegaard, K., Rannik, U., Rebmann, C., Suyker, A., Tenhunen, J., Tu, K., Verma,
495 S., Vesala, T., Wilson, K., and Wofsy, S.: Gap filling strategies for defensible annual sums of net
496 ecosystem exchange, Agric. For. Meteorol., 107, 43-69, 2001.
497 Farquhar, G. D., Caemmerer, S., and Berry, J. A.: A biochemical model of photosynthetic CO_2
498 assimilation in leaves of C3 plants, Planta, 149, 78-90, 1980.
499 Fensholt, R., and Sandholt, I.: Derivation of a shortwave infrared water stress index from MODIS
500 near- and shortwave infrared data in a semiarid environment, Remote Sens. Environ., 87, 111-121,
501 http://dx.doi.org/10.1016/j.rse.2003.07.002, 2003.
502 Fensholt, R., Sandholt, I, Rasmussen, M. S., Stisen, S., and Diouf, A.: Evaluation of satellite based
503 primary production modelling in the semi-arid Sahel, Remote Sens. Environ., 105, 173-188,
504 10.1016/j.rse.2006.06.011, 2006a.
505 Fensholt, R., Sandholt, I., and Stisen, S.: Evaluating MODIS, MERIS, and VEGETATION
506 vegetation indices using in situ measurements in a semiarid environment, IEEE T. Geosci. Remote,
507 44, 1774-1786, 10.1109/TGRS.2006.875940, 2006b.
508 Fensholt, R., Rasmussen, K., Kaspersen, P., Huber, S., Horion, S., and Swinnen, E.: Assessing Land
509 Degradation/Recovery in the African Sahel from Long-Term Earth Observation Based Primary
510 Productivity and Precipitation Relationships, Remote Sensing, 5, 664-686, 2013.
511 Garbulsky, M. F., Peñuelas, J., Papale, D., Ardö, J., Goulden, M. L., Kiely, G., Richardson, A. D.,
512 Rotenberg, E., Veenendaal, E. M., and Filella, I.: Patterns and controls of the variability of radiation
513 use efficiency and primary productivity across terrestrial ecosystems, Global Ecol. Biogeogr., 19,
514 253-267, 10.1111/j.1466-8238.2009.00504.x, 2010.
515 Gates, D. M., Keegan, H. J., Schleter, J. C., and Weidner, V. R.: Spectral Properties of Plants, Appl.
516 Optics, 4, 11-20, 1965.
517 Gebremichael, M., and Barros, A. P.: Evaluation of MODIS Gross Primary Productivity (GPP) in
518 tropical monsoon regions, Remote Sens. Environ., 100, 150-166,
519 http://dx.doi.org/10.1016/j.rse.2005.10.009, 2006.
520 Haboudane, D., Miller, J. R., Pattey, E., Zarco-Tejada, P. J., and Strachan, I. B.: Hyperspectral
521 vegetation indices and novel algorithms for predicting green LAI of crop canopies: Modeling and
522 validation in the context of precision agriculture, Remote Sens. Environ., 90, 337-352,
523 http://dx.doi.org/10.1016/j.rse.2003.12.013, 2004.
524 Heinsch, F. A., Maosheng, Z., Running, S. W., Kimball, J. S., Nemani, R. R., Davis, K. J., Bolstad,
525 P. V., Cook, B. D., Desai, A. R., Ricciuto, D. M., Law, B. E., Oechel, W. C., Hyojung, K., Hongyan,
526 L., Wofsy, S. C., Dunn, A. L., Munger, J. W., Baldocchi, D. D., Liukang, X., Hollinger, D. Y.,
527 Richardson, A. D., Stoy, P. C., Siqueira, M. B. S., Monson, R. K., Burns, S. P., and Flanagan, L. B.:
528 Evaluation of remote sensing based terrestrial productivity from MODIS using regional tower eddy
529 flux network observations, IEEE T. Geosci. Remote, 44, 1908-1925, 10.1109/TGRS.2005.853936,
530 2006.
531 Hickler, T., Eklundh, L., Seaquist, J. W., Smith, B., Ardö, J., Olsson, L., Sykes, M. T., and
532 Sjostrom, M.: Precipitation controls Sahel greening trend, Geophys. Res. Lett., 32, L21415,
533 doi:10.1029/2005GL024370, 2005.
534 Huber, S., Tagesson, T., and Fensholt, R.: An automated field spectrometer system for studying
535 VIS, NIR and SWIR anisotropy for semi-arid savanna, Remote Sens. Environ., 152, 547–556, 2014.
536 Huete, A., Didan, K., Miura, T., Rodriguez, E. P., Gao, X., and Ferreira, L. G.: Overview of the
537 radiometric and biophysical performance of the MODIS vegetation indices, Remote Sens. Environ.,
538 83, 195–213, 2002.

539 Ide, R., Nakaji, T., and Oguma, H.: Assessment of canopy photosynthetic capacity and estimation
540 of GPP by using spectral vegetation indices and the light-response function in a larch forest, Agric.
541 For. Meteorol., 150, 389-398, 2010.
542 Inoue, Y., Penuelas, J., Miyata, A., and Mano, M.: Normalized difference spectral indices for
543 estimating photosynthetic efficiency and capacity at a canopy scale derived from hyperspectral and
544 CO_2 flux measurements in rice, Remote Sens. Environ., 112, 156-172, 2008.
545 Jin, H., and Eklundh, L.: A physically based vegetation index for improved monitoring of plant
546 phenology, Remote Sens. Environ., 152, 512-525, http://dx.doi.org/10.1016/j.rse.2014.07.010, 2014.
547 Kanniah, K. D., Beringer, J., Hutley, L. B., Tapper, N. J., and Zhu, X.: Evaluation of Collections 4
548 and 5 of the MODIS Gross Primary Productivity product and algorithm improvement at a tropical
549 savanna site in northern Australia, Remote Sens. Environ., 113, 1808-1822,
550 http://dx.doi.org/10.1016/j.rse.2009.04.013, 2009.
551 Kergoat, L., Lafont, S., Arneth, A., Le Dantec, V., and Saugier, B.: Nitrogen controls plant canopy
552 light-use efficiency in temperate and boreal ecosystems, J. Geophys. Res., 113, n/a-n/a,
553 10.1029/2007JG000676, 2008.
554 Leblanc, M. J., Favreau, G., Massuel, S., Tweed, S. O., Loireau, M., and Cappelaere, B.: Land
555 clearance and hydrological change in the Sahel: SW Niger, Global Planet. Change, 61, 135-150,
556 http://dx.doi.org/10.1016/j.gloplacha.2007.08.011, 2008.
557 Ma, X., Huete, A., Yu, Q., Restrepo-Coupe, N., Beringer, J., Hutley, L. B., Kanniah, K. D.,
558 Cleverly, J., and Eamus, D.: Parameterization of an ecosystem light-use-efficiency model for
559 predicting savanna GPP using MODIS EVI, Remote Sens. Environ., 154, 253-271,
560 http://dx.doi.org/10.1016/j.rse.2014.08.025, 2014.
561 Mayaux, P., Bartholomé, E., Massart, M., Cutsem, C. V., Cabral, A., Nonguierma, A., Diallo, O.,
562 Pretorius, C., Thompson, M., Cherlet, M., Pekel, J.-F., Defourny, P., Vasconcelos, M., Gregorio, A.
563 D., S.Fritz, Grandi, G. D., C..Elvidge, P.Vogt, and Belward, A.: EUR 20665 EN –A Land-cover
564 map of Africa, edited by: Centre', E. C. J. R., European Commisions Joint Research Centre,
565 Luxembourg, 38 pp., 2003.
566 Mbow, C., Fensholt, R., Rasmussen, K., and Diop, D.: Can vegetation productivity be derived from
567 greenness in a semi-arid environment? Evidence from ground-based measurements, J. Arid
568 Environ., 97, 56-65, http://dx.doi.org/10.1016/j.jaridenv.2013.05.011, 2013.
569 Moncrieff, J. B., Monteny, B., Verhoef, A., Friborg, T., Elbers, J., Kabat, P., de Bruin, H., Soegaard,
570 H., Jarvis, P. G., and Taupin, J. D.: Spatial and temporal variations in net carbon flux during
571 HAPEX-Sahel, J. Hydrol., 188–189, 563-588, 10.1016/s0022-1694(96)03193-9, 1997.
572 Monteith, J. L.: Solar radiation and productivity in tropical ecosystems, J. Appl. Ecol., 9, 747-766,
573 1972.
574 Monteith, J. L.: Climate and the efficiency of crop production in Britain, Philos. Trans. Roy. Soc. B.,
575 281, 277-294, 1977.
576 Mutanga, O., and Skidmore, A. K.: Narrow band vegetation indices overcome the saturation
577 problem in biomass estimation, Int. J. Remote Sens., 25, 3999-4014,
578 10.1080/01431160310001654923, 2004.
579 NASA: Reverb ECHO: http://reverb.echo.nasa.gov/reverb/, access: June 2016, 2016.
580 Papale, D., Reichstein, M., Aubinet, M., Canfora, E., Bernhofer, C., Kutsch, W., Longdoz, B.,
581 Rambal, S., Valentini, R., Vesala, T., and Yakir, D.: Towards a standardized processing of Net
582 Ecosystem Exchange measured with eddy covariance technique: algorithms and uncertainty
583 estimation, Biogeosciences, 3, 571-583, 10.5194/bg-3-571-2006, 2006.
584 Paruelo, J. M., Garbulsky, M. F., Guerschman, J. P., and Jobbágy, E. G.: Two decades of
585 Normalized Difference Vegetation Index changes in South America: identifying the imprint of
586 global change, Int. J. Remote Sens., 25, 2793-2806, 10.1080/01431160310001619526, 2004.

Biogeosciences Open Access

Discussions EGU

587 Poulter, B., Frank, D., Ciais, P., Myneni, R. B., Andela, N., Bi, J., Broquet, G., Canadell, J. G.,
588 Chevallier, F., Liu, Y. Y., Running, S. W., Sitch, S., and van der Werf, G. R.: Contribution of semi-
589 arid ecosystems to interannual variability of the global carbon cycle, Nature, 509, 600-603,
590 10.1038/nature13376, 2014.
591 Prince, S. D., Kerr, Y. H., Goutorbe, J. P., Lebel, T., Tinga, A., Bessemoulin, P., Brouwer, J.,
592 Dolman, A. J., Engman, E. T., Gash, J. H. C., Hoepffner, M., Kabat, P., Monteny, B., Said, F.,
593 Sellers, P., and Wallace, J.: Geographical, biological and remote sensing aspects of the hydrologic
594 atmospheric pilot experiment in the sahel (HAPEX-Sahel), Remote Sens. Environ., 51, 215-234,
595 http://dx.doi.org/10.1016/0034-4257(94)00076-Y, 1995.
596 Qi, J., Chehbouni, A., Huete, A. R., Kerr, Y. H., and Sorooshian, S.: A modified soil adjusted
597 vegetation index, Remote Sens. Environ., 48, 119-126, 1994.
598 Richter, K., Atzberger, C., Hank, T. B., and Mauser, W.: Derivation of biophysical variables from
599 Earth observation data: validation and statistical measures, J. Appl. Remote Sens., 6, 063557,
600 10.1117/1.JRS.6.063557, 2012.
601 Rietkerk, M., Ketner, P., Stroosnijder, L., and Prins, H. H. T.: Sahelian rangeland development; a
602 catastrophe?, J. Range Manage., 49, 512-519, 1996.
603 Rockström, J., and de Rouw, A.: Water, nutrients and slope position in on-farm pearl millet
604 cultivation in the Sahel, Plant Soil, 195, 311-327, 10.1023/A:1004233303066, 1997.
605 Roujean, J.-L., and Breon, F.-M.: Estimating PAR absorbed by vegetation from bidirectional
606 reflectance measurements, Remote Sens. Environ., 51, 375-384, http://dx.doi.org/10.1016/0034-
607 4257(94)00114-3, 1995.
608 Rouse, J. W., Haas, R. H., Schell, J. A., Deering, D. W., and Harlan, J. C.: Monitoring the Vernal
609 Advancement of Retrogradation of Natural Vegetation, Type III, Final Report, Greenbelt, MD,
610 1974.
611 Ruimy, A., Saugier, B., and Dedieu, G.: Methodology for the estimation of terrestrial net primary
612 production from remotely sensed data., J. Geophys. Res., 99, 5263-5283., 1994.
613 Running, S. W., Nemani, R. R., Heinsch, F. A., Zhao, M., Reeves, M., and Hashimoto, H.: A
614 Continuous Satellite-Derived Measure of Global Terrestrial Primary Production, BioScience, 54,
615 547-560, 10.1641/0006-3568(2004)054[0547:ACSMOG]2.0.CO;2, 2004.
616 Running, S. W., and Zhao, M.: User's Guide. Daily GPP and Annual NPP (MOD17A2/A3)
617 Products NASA Earth Observing System MODIS Land Algorithm. Version 3.0 For Collection 6.,
618 University of Montana, USA, NASA, 2015.
619 Samaké, O., Smaling, E. M. A., Kropff, M. J., Stomph, T. J., and Kodio, A.: Effects of cultivation
620 practices on spatial variation of soil fertility and millet yields in the Sahel of Mali, Agr. Ecosyst.
621 Environ., 109, 335-345, http://dx.doi.org/10.1016/j.agee.2005.02.024, 2005.
622 Scholes, R. J., and Archer, S. R.: Tree-grass interactions in savannas, Annual Review of Ecology
623 and Systematics, 28, 517-544, 1997.
624 Sellers, P. J., Dickinson, R. E., Randall, D. A., Betts, A. K., Hall, F. G., Berry, J. A., Collatz, G. J.,
625 Denning, A. S., Mooney, H. A., Nobre, C. A., Sato, N., Field, C. B., and Henderson-Sellers, A.:
626 Modeling the Exchanges of Energy, Water, and Carbon Between Continents and the Atmosphere,
627 Science, 275, 502-509, 10.1126/science.275.5299.502, 1997.
628 Sims, D. A., Rahman, A. F., Cordova, V. D., El-Masri, B. Z., Baldocchi, D. D., Flanagan, L. B.,
629 Goldstein, A. H., Hollinger, D. Y., Misson, L., Monson, R. K., Oechel, W. C., Schmid, H. P.,
630 Wofsy, S. C., and Xu, L.: On the use of MODIS EVI to assess gross primary productivity of North
631 American ecosystems, J. Geophys. Res., 111, G04015, 10.1029/2006JG000162, 2006.
632 Sjöström, M., Ardö, J., Eklundh, L., El-Tahir, B. A., El-Khidir, H. A. M., Hellström, M., Pilesjö, P.,
633 and Seaquist, J.: Evaluation of satellite based indices for gross primary production estimates in a
634 sparse savanna in the Sudan, Biogeosciences, 6, 129-138, 2009.

635 Sjöström, M., Zhao, M., Archibald, S., Arneth, A., Cappelaere, B., Falk, U., de Grandcourt, A.,
636 Hanan, N., Kergoat, L., Kutsch, W., Merbold, L., Mougin, E., Nickless, A., Nouvellon, Y., Scholes,
637 R. J., Veenendaal, E. M., and Ardö, J.: Evaluation of MODIS gross primary productivity for Africa
638 using eddy covariance data, Remote Sens. Environ., 131, 275-286,
639 http://dx.doi.org/10.1016/j.rse.2012.12.023, 2013.
640 Tagesson, T., Eklundh, L., and Lindroth, A.: Applicability of leaf area index products for boreal
641 regions of Sweden, Int. J. Remote Sens., 30, 5619–5632, 2009.
642 Tagesson, T., Fensholt, R., Cropley, F., Guiro, I., Horion, S., Ehammer, A., and Ardö, J.: Dynamics
643 in carbon exchange fluxes for a grazed semi-arid savanna ecosystem in West Africa, Agr. Ecosyst.
644 Environ., 205, 15-24, http://dx.doi.org/10.1016/j.agee.2015.02.017, 2015a.
645 Tagesson, T., Fensholt, R., Guiro, I., Rasmussen, M. O., Huber, S., Mbow, C., Garcia, M., Horion,
646 S., Sandholt, I., Rasmussen, B. H., Göttsche, F. M., Ridler, M.-E., Olén, N., Olsen, J. L., Ehammer,
647 A., Madsen, M., Olesen, F. S., and Ardö, J.: Ecosystem properties of semi-arid savanna grassland in
648 West Africa and its relationship to environmental variability, Global Change Biol., 21, 250-264, doi:
649 10.1111/gcb.12734, 2015b.
650 Tagesson, T., Fensholt, R., Huber, S., Horion, S., Guiro, I., Ehammer, A., and Ardö, J.: Deriving
651 seasonal dynamics in ecosystem properties of semi-arid savannas using in situ based hyperspectral
652 reflectance, Biogeosciences, 12, 4621-4635, doi:10.5194/bg-12-4621-2015, 2015c.
653 Tagesson, T., Fensholt, R., Cappelaere, B., E., M., Horion, S., L., K., Nieto, H., Ehammer, A.,
654 Demarty, J., and Ardö, J.: Spatiotemporal variability in carbon exchange fluxes across the Sahel
655 Agric. For. Meteorol., 226–227, 108-118, 2016.
656 Timouk, F., Kergoat, L., Mougin, E., Lloyd, C. R., Ceschia, E., Cohard, J. M., Rosnay, P. d.,
657 Hiernaux, P., Demarez, V., and Taylor, C. M.: Response of surface energy balance to water regime
658 and vegetation development in a Sahelian landscape, J. Hydrol., 375, 12-12,
659 10.1016/j.jhydrol.2009.04.022, 2009.
660 Turner, D. P., Ritts, W. D., Cohen, W. B., Maeirsperger, T. K., Gower, S. T., Kirschbaum, A. A.,
661 Running, S. W., Zhao, M., Wofsy, S. C., Dunn, A. L., Law, B. E., Campbell, J. L., Oechel, W. C.,
662 Kwon, H. J., Meyers, T. P., Small, E. E., Kurc, S. A., and Gamon, J. A.: Site-level evaluation of
663 satellite-based global terrestrial gross primary production and net primary production monitoring,
664 Global Change Biol., 11, 666-684, 2005.
665 Turner, D. P., Ritts, W. D., and Cohen, W. B.: Evaluation of MODIS NPP and GPP products across
666 multiple biomes, Remote Sens. Environ., 102, 282-293, 2006.
667 United Nations: Sahel Regional Strategy Mid-Year Review 2013 New York, 1-59, 2013.
668 Velluet, C., Demarty, J., Cappelaere, B., Braud, I., Issoufou, H. B. A., Boulain, N., Ramier, D.,
669 Mainassara, I., Charvet, G., Boucher, M., Chazarin, J. P., Oï, M., Yahou, H., Maidaji, B., Arpin-
670 Pont, F., Benarrosh, N., Mahamane, A., Nazoumou, Y., Favreau, G., and Seghieri, J.: Building a
671 field- and model-based climatology of local water and energy cycles in the cultivated Sahel; annual
672 budgets and seasonality, Hydrol. Earth Syst. Sci., 18, 5001-5024, 10.5194/hess-18-5001-2014, 2014.
673 Wall, G. W., and Kanemasu, E. T.: Carbon dioxide exchange rates in wheat canopies. Part I.
674 Influence of canopy geometry on trends in leaf area index, light interception and instantaneous
675 exchange rates, Agric. For. Meteorol., 49, 81-102, http://dx.doi.org/10.1016/0168-1923(90)90044-7,
676 1990.
677 Yoder, B. J., and Pettigrew-Crosby, R. E.: Predicting nitrogen and chlorophyll content and
678 concentrations from reflectance spectra (400–2500 nm) at leaf and canopy scales, Remote Sens.
679 Environ., 53, 199-211, http://dx.doi.org/10.1016/0034-4257(95)00135-N, 1995.
680 Zhang, Y., Guanter, L., Berry, J. A., Joiner, J., van der Tol, C., Huete, A., Gitelson, A., Voigt, M.,
681 and Köhler, P.: Estimation of vegetation photosynthetic capacity from space-based measurements

682   of chlorophyll fluorescence for terrestrial biosphere models, Global Change Biol., 20, 3727-3742,

683   10.1111/gcb.12664, 2014.

684

685

686 **Tables**

687 **Table 1.** Description of the six measurement sites including location, soil type, ecosystem type and dominant species.

Measurement site	Coordinates	Soil type	Ecosystem	Dominant species
Agoufou[a] (ML-AgG, Mali)	15.34°N, 1.48°W	Sandy ferruginous Arenosol	Open woody savannah (4% tree cover)	Trees: *Acacia spp., Balanites aegyptiaca, Combretum glutinosum* *Herbs: Zornia glochidiata, Cenchrus biflorus, Aristida mutabilis, Tragus berteronianus*
Dahra[b] (SN-Dah, Senegal)	15.40°N, 15.43°W	Sandy luvic arenosol	Grassland/shrubland Savanna (3% tree cover)	Trees: *Acacia spp., Balanites aegyptiaca* Herbs: *Zornia latifolia, Aristida adscensionis, Cenchrus biflorus*
Demokeya[c] (SD-Dem, Sudan)	13.28°N, 30.48°E	Cambic Arenosol	Sparse acacia savannah (7% tree cover)	*Trees: Acacia spp.,* Herbs: *Aristida pallida, Eragrostis tremula, Cenchrus biflorus*
Kelma[a] (ML-Kem, Mali)	15.22°N, 1.57°W	Clay soil depression	Open acacia forest (90% tree cover)	Trees: *Acacia seyal, Acacia nilotica, Balanites aegyptiaca* Herbs: *Sporobolus hevolvus, Echinochloa colona, Aeschinomene sensitive*
Wankama Fallow[d] (NE-WaF, Niger)	13.65°N, 2.63°E	Sandy ferruginous Arenosol	Fallow bush	*Guiera senegalensis*
Wankama Millet[e] (NE-WaM, Niger)	13.64°N, 2.63°E	Sandy ferruginous Arenosol	Millet crop	*Pennisetum glaucum*

688 [a](Timouk et al., 2009)
689 [b](Tagesson et al., 2015b)
690 [c](Sjöström et al., 2009)
691 [d](Velluet et al., 2014)
692 [e](Boulain et al., 2009)

Table 2. Correlation between dynamics in photosynthetic capacity (F_{opt}), quantum efficiency (α), and the different vegetation indices for the six measurement sites (Fig. 1). Values are averages±1 standard deviation from 200 bootstraping runs. The bold values are the indices with the strongest correlation. EVI is the enhanced vegetation index, NDVI is the normalized difference vegetation index, RDVI is the renormalized difference vegetation index, SIWSI is the shortwave infrared water stress index. $SIWSI_{12}$ is based on the MODIS Bidirectional Reflectance Distribution Functions (NBAR) band 2 and band 5, whereas $SIWSI_{16}$ is based on MODIS NBAR band 2 and band 6.

Measurement site	F_{opt}					α				
	EVI	NDVI	RDVI	$SIWSI_{12}$	$SIWSI_{16}$	EVI	NDVI	RDVI	$SIWSI_{12}$	$SIWSI_{16}$
ML-AgG	0.89±0.02	0.87±0.02	0.95±0.01	**-0.95±0.01**	-0.93±0.02	0.92±0.02	0.91±0.01	**0.96±0.01**	-0.94±0.01	-0.88±0.02
SN-Dah	0.92±0.005	0.91±0.01	0.96±0.003	**-0.96±0.004**	-0.93±0.01	0.89±0.01	0.90±0.01	**0.93±0.01**	-0.92±0.01	-0.87±0.01
SD-Dem	0.81±0.01	0.78±0.01	0.91±0.01	**-0.93±0.01**	-0.90±0.01	0.76±0.02	0.73±0.02	**0.86±0.01**	-0.82±0.02	-0.79±0.02
MA-Kem	0.77±0.02	0.83±0.02	0.95±0.01	**-0.95±0.01**	-0.90±0.02	0.69±0.05	0.73±0.04	**0.80±0.03**	-0.77±0.03	-0.76±0.03
NE-WaF	0.87±0.02	0.81±0.02	0.78±0.02	**-0.90±0.01**	-0.80±0.02	**0.89±0.01**	0.84±0.01	0.85±0.01	-0.88±0.01	-0.79±0.01
NE-WaM	0.41±0.05	0.50±0.04	0.72±0.03	-0.55±0.04	-0.43±0.05	0.72±0.02	0.76±0.02	**0.81±0.01**	-0.75±0.01	-0.72±0.01
All sites	0.86±0.0	0.79±0.0	**0.90±0.0**	0.75±0.0	0.70±0.0	0.83±0.01	0.80±0.01	**0.86±0.01**	0.62±0.01	0.54±0.01

Table 3. Statistics for the regression tree analysis studying relationships between intra-annual dynamics in the the photosynthetic capacity (F_{opt}) and quantum efficiency (α) and the explanatory variables for the six measurement sites (Fig. 1). The pruning level is the number of splits of the regression tree and an indication of complexity of the system.

Measurement site	Explanatory variables:					Pruning level	R^2
F_{opt}	1	2	3	4	5		
ML-AgG	$SIWSI_{12}$	Tair	PAR	SWC		16	0.98
SN-Dah	$SIWSI_{12}$	SWC	VPD	Tair	PAR	84	0.98
SD-Dem	$SIWSI_{12}$	VPD	SWC	Tair	PAR	33	0.97
ML-Kem	$SIWSI_{12}$	PAR	Tair	VPD		22	0.98
NE-WaF	$SIWSI_{12}$	SWC	VPD	Tair		14	0.92
NE-WaM	RDVI	SWC	VPD	Tair		18	0.75
All sites	RDVI	SWC	Tair	VPD		16	0.87
α							
ML-AgG	RDVI					3	0.95
SN-Dah	RDVI	VPD	SWC	Tair	PAR	21	0.93
SD-Dem	RDVI	SWC	PAR	Tair		16	0.93
ML-Kem	RDVI	Tair				4	0.75
NE-WaF	EVI	SWC	VPD			10	0.90
NE-WaM	RDVI	SWC	VPD	Tair		15	0.86
All sites	RDVI	SWC	VPD	Tair		16	0.84

Table 4. Annual peak values of quantum efficiency (α_{peak}; μmol CO_2 μmol PAR^{-1}) and photosynthetic capacity (F_{opt_peak}; μmol CO_2 m^{-2} s^{-1}) for the six measurement sites (Fig. 1). The peak values are the 2 week running mean with highest annual value.

Measurement site	Year	α_{peak}	F_{opt_peak}
ML-AgG	2007	0.0396	24.5
SN-Dah	2010	0.0638	50.0
	2011	0.0507	42.3
	2012	0.0480	39.2
	2013	0.0549	40.0
SD-Dem	2007	0.0257	16.5
	2008	0.0327	21.0
	2009	0.0368	16.5
ML-Kem	2007	0.0526	33.5
NE-WaF	2005	0.0273	18.2
	2006	0.0413	21.0
NE-WaM	2005	0.0252	10.6
	2006	0.0200	10.1
Average		0.0399	26.4

Table 5. Correlation matrix between annual peak values of photosynthetic capacity (F_{opt_peak}) and quantum efficiency (α_{peak}) and measured environmental variables. P is annual rainfall; T_{air} is yearly averaged air temperature at 2 m height; SWC is yearly averaged soil water content (% volumetric water content) measured at 0.1 m depth; Rh is yearly averaged relative humidity; VPD is yearly averaged vapour pressure deficit; R_g is yearly averaged incoming global radiation; N and C cont. are soil nitrogen and carbon contents; $NDVI_{peak}$ is annual peak normalized difference vegetation index (NDVI); EVI_{peak} is annual peak enhanced vegetation index (EVI); $RDVI_{peak}$ is annual peak renormalized difference vegetation index (RDVI); $SIWSI_{12peak}$ is annual peak short wave infrared water stress index based on MODIS NBAR band 2 and band 5; and $SIWSI_{16peak}$ is annual peak short wave infrared water stress index based on MODIS NBAR band 2 and band 6. Sample size was 13 for all except the marked explanatory variables.

Explanatory variable	F_{opt_peak}	α_{peak}
Meteorological data		
P (mm)	0.24±0.26	0.13±0.27
T_{air} (°C)	-0.07±0.25	-0.01±0.25
SWC (%)[a]	0.33±0.25	0.16±0.27
Rh (%)	0.73±0.16[*]	0.60±0.19
VPD (hPa)	0.20±0.26	0.15±0.30
R_g (W m^{-2})	-0.48±0.21	-0.41±0.24
Biomass and edaphic data		
Biomass (g DW m^{-2})[a]	0.77±0.15[*]	0.74±0.14[*]
C3/C4 ratio	-0.05±0.26	0.06±0.30
N cont. (%)[b]	0.22±0.11	0.35±0.14
C cont. (%)[b]	0.89±0.06[**]	0.87±0.07[**]
Earth observation data		
$NDVI_{peak}$	0.94±0.05[**]	0.87±0.07[*][**]
EVI_{peak}	0.93±0.04[**]	0.87±0.07[**]
$RDVI_{peak}$	0.93±0.04[**]	0.89±0.07[**]
$SIWSI_{12peak}$	0.85±0.08[**]	0.84±0.08[**]
$SIWSI_{16peak}$	0.67±0.12[*]	0.65±0.15[*]
Photosynthetic variables		
F_{opt}	-	0.94±0.03[**]

[a]sample size equals 11.
[b]sample size equals 9.
* significant at 0.05 level.
** significant at 0.01 level

Table 6. Statistics regarding the evaluation of the gross primary productivity (GPP) model for the six measurement sites (Fig. 1). In situ and modelled GPP are averages ± 1 standard deviation. RMSE is the root-mean-squares-error, and slope, intercept and R^2 is from the fitted ordinary least squares linear regression.

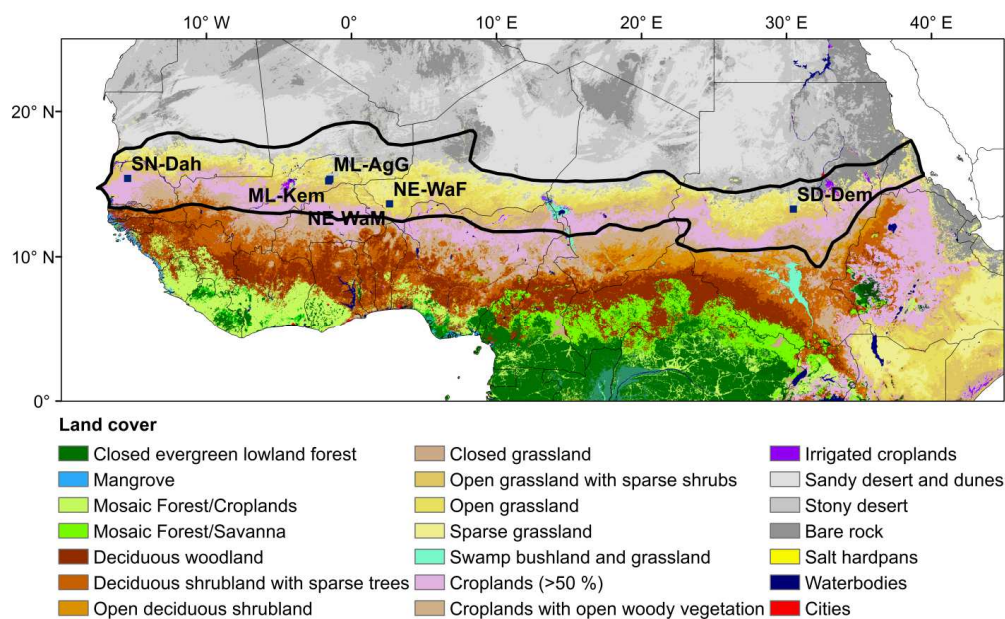| Measurement site	In situ GPP ($\mu mol\ CO_2\ m^{-2}\ s^{-1}$)	Modelled GPP ($\mu mol\ CO_2\ m^{-2}\ s^{-1}$)	RMSE ($\mu mol\ CO_2\ m^{-2}\ s^{-1}$)	slope	Intercept ($\mu mol\ CO_2\ m^{-2}\ s^{-1}$)	R^2
ML-AgG	3.55±5.45	3.91±5.54	1.83±0.10	0.97±0.06	0.50±0.03	0.90±0.01
SN-Dah	9.14±10.12	8.60±10.72	3.85±1.34	0.99±0.07	-0.44±1.11	0.87±0.04
SD-Dem	3.83±4.42	3.61±4.51	3.05±1.06	0.79±0.18	0.61±0.75	0.59±0.11
ML-Kem	11.17±7.98	10.73±10.50	5.06±1.23	1.16±0.20	-2.29±1.65	0.79±0.12
NE-WaF	3.91±4.08	5.38±3.97	2.55±1.05	0.85±0.15	2.08±1.48	0.75±0.08
NE-WaM	2.25±2.00	5.51±3.93	4.13±0.99	1.63±0.45	1.84±1.01	0.68±0.05
Average	5.31±7.15	5.80±7.53	3.56±0.60	0.94±0.07	0.85±0.92	0.84±0.08

Table 7. The parameters for Eq. 18 that was used in the final gross primary productivity (GPP) model. RMSE is the root mean square error, and R^2 is the coefficient of determination of the linear regression models predicting the different variables.

Parameter	Value	RMSE	R^2
k_{Fopt}	79.6±6.3	5.1±1.3	0.89±0.05
m_{Fopt}	-7.3±3.2		
l_{Fopt}	1.81±0.07	0.33±0.04	0.79±0.04
n_{Fopt}	-0.85±0.07		
k_{α}	0.16±0.02	0.0069±0.0021	0.81±0.10
m_{α}	-0.014±0.007		
l_{α}	1.20±0.05	0.38±0.04	0.71±0.04
n_{α}	-0.98±0.06		

5

Figures

Figure 1. Land use cover classes for the Sahel and the location of the six measurement sites included in the study. The land cover classes are based on multi-sensor satellite observations (Mayaux et al., 2003). The sites are Agoufou (ML-AgG), Dahra (SN-Dah), Demokeya (SD-Dem), Kelma (ML-Kem), Wankama Fallow (NE-WaF), and Wankama Millet (NE-WaM). The thick black line is the borders of the Sahel based on the isohytes 150 and 700 mm of annual precipitation (Prince et al., 1995)
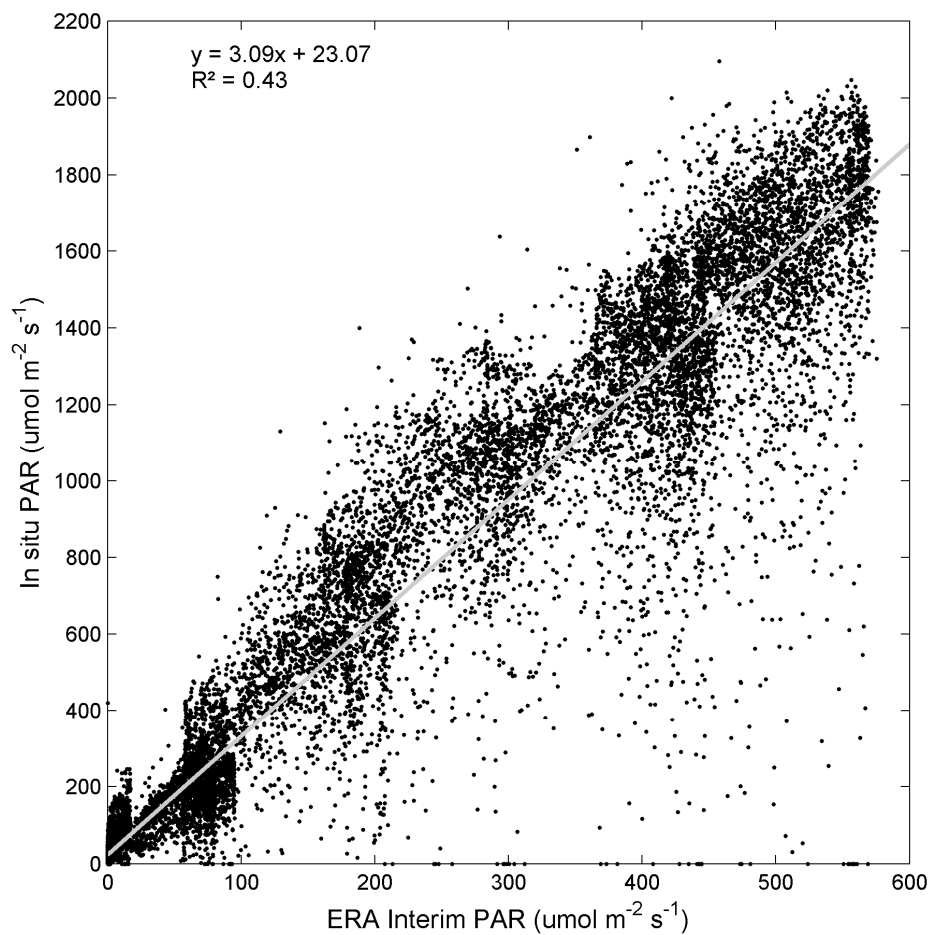
Biogeosciences
Discussions

Open Access

EGU

Figure 2. Photosynthetically active radiation (PAR) measured in situ against gridded ERA Interim ground surface PAR extracted for the six measurement sites (Figure 1) across the Sahel from European Centre for Medium-Range Weather Forecasts, ECMWF (2016). The grey line is the ordinary least square linear regression.
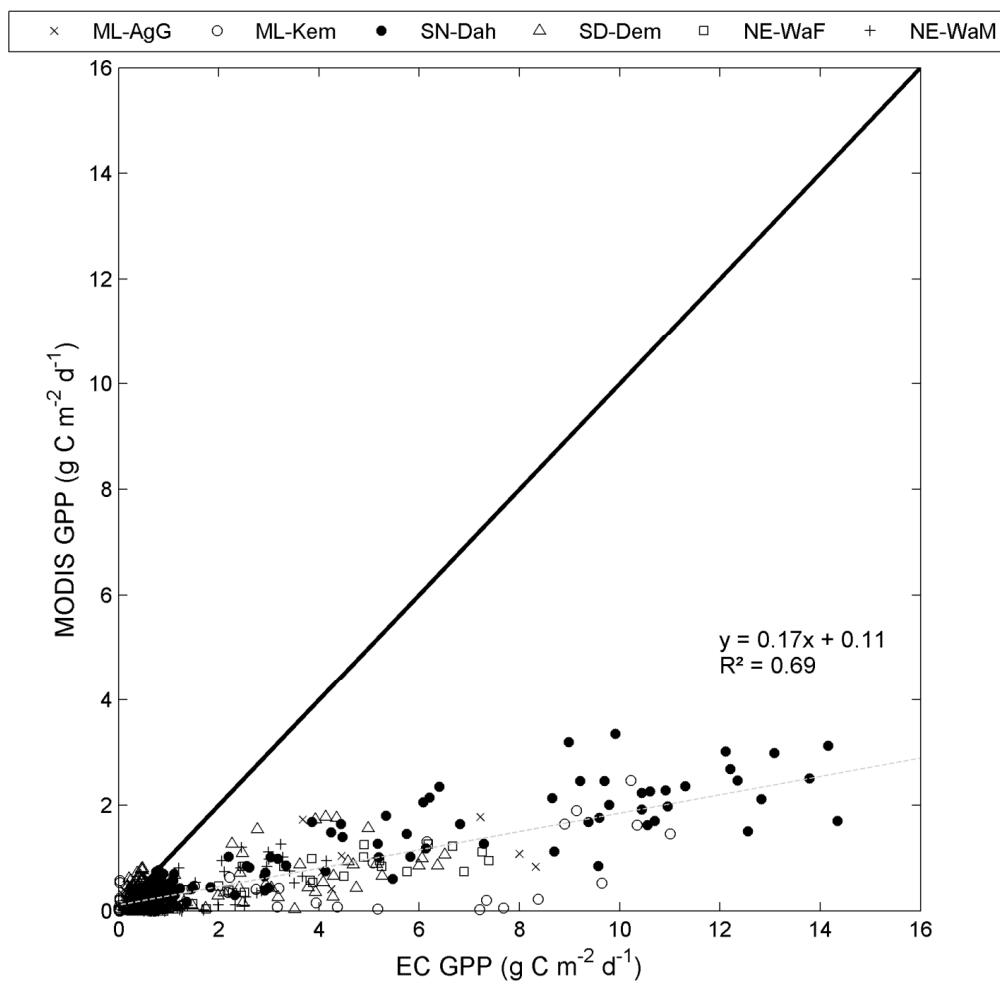
5

Figure 3. Evaluation of the MODIS based GPP product MOD17A2H collection 6 against eddy covariance based GPP from the six measurement sites (Figure 1) across the Sahel. The thick black line shows the one-to-one ratio, and the thin grey dotted line is the fitted ordinary least square linear regression.
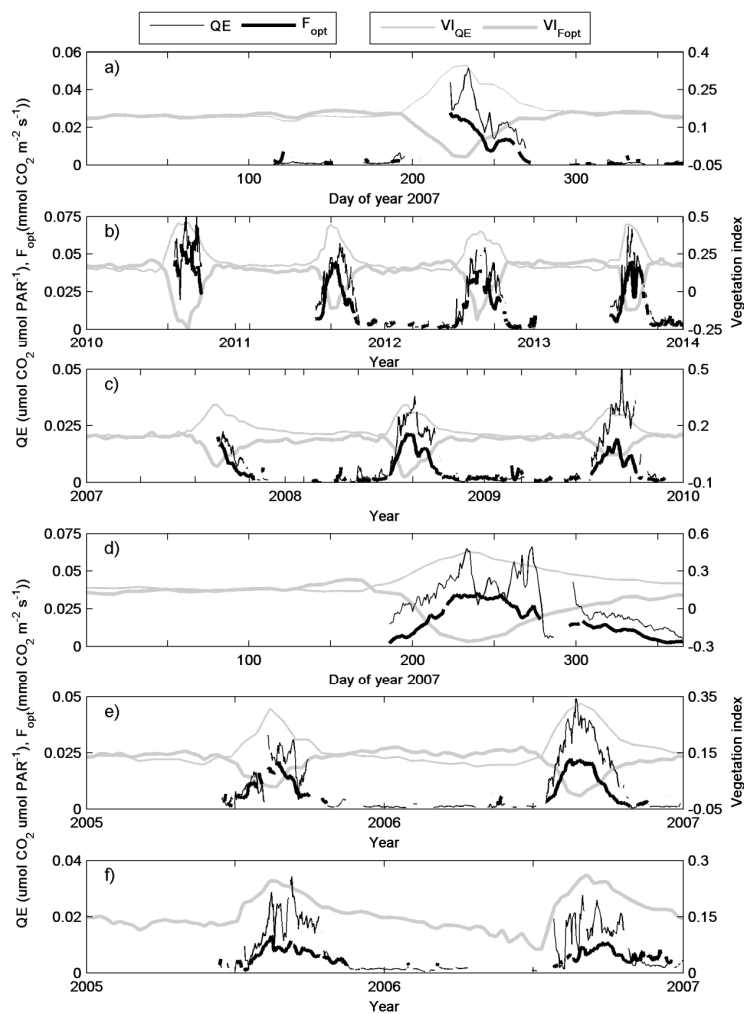
5

Figure 4. Dynamics in photosynthetic capacity (F_{opt}) and quantum efficiency (QE, α) for the six measurement sites. Included is also dynamics in the vegetation indices with highest correlation to the intra-annual dynamics in Fopt (VI_{Fopt}) and to quantum efficiency (VI_{QE}) (Table 2). The sites are a) Agoufou (ML-AgG), b) Dahra (SN-Dah), c) Demokeya (SD-Dem), d) Kelma (ML-Kem), e) Wankama Fallow (NE-WaF), and f) Wankama Millet (NE-WaM).
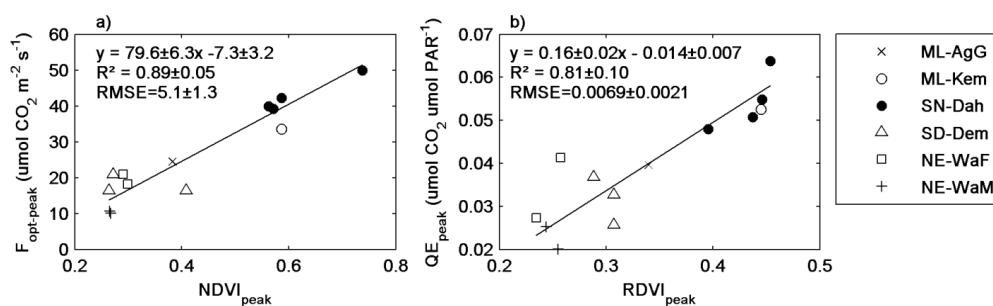
Biogeosciences

Open Access

Discussions

EGU

Figure 5. Scatter plots of annual peak values for the six measurement sites (Figure 1) of a) photosynthetic capacity (F_{opt_peak})
5   and b) quantum efficiency (QE_{peak}; α_{peak}) against peak values of normalized difference vegetation index ($NDVI_{peak}$) and
renormalized difference vegetation index ($RDVI_{peak}$), respectively. The annual peak values were estimated by taking the
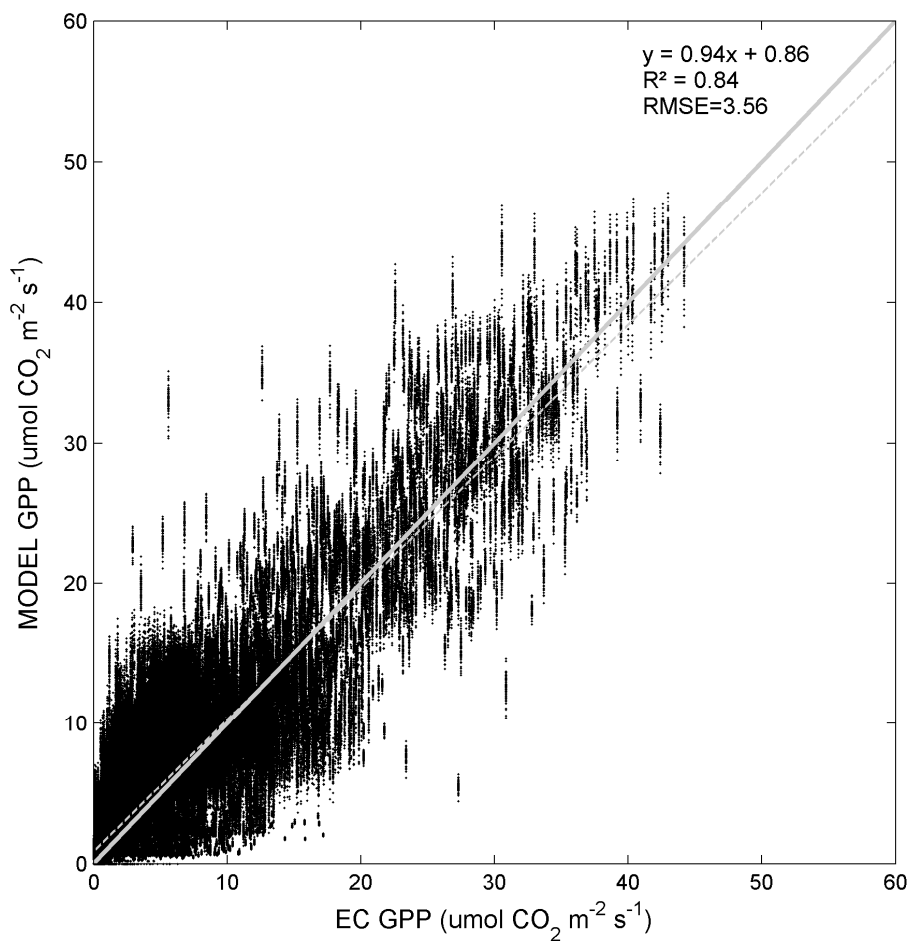annual maximum of a two week running mean.

Figure 6. Evaluation of the modelled gross primary productivity (GPP) (Eq. 18) against in situ GPP from all six measurement sites across the Sahel. The thick grey line shows the one-to-one ratio, whereas the dotted thin grey line is the fitted ordinary least square linear regression.
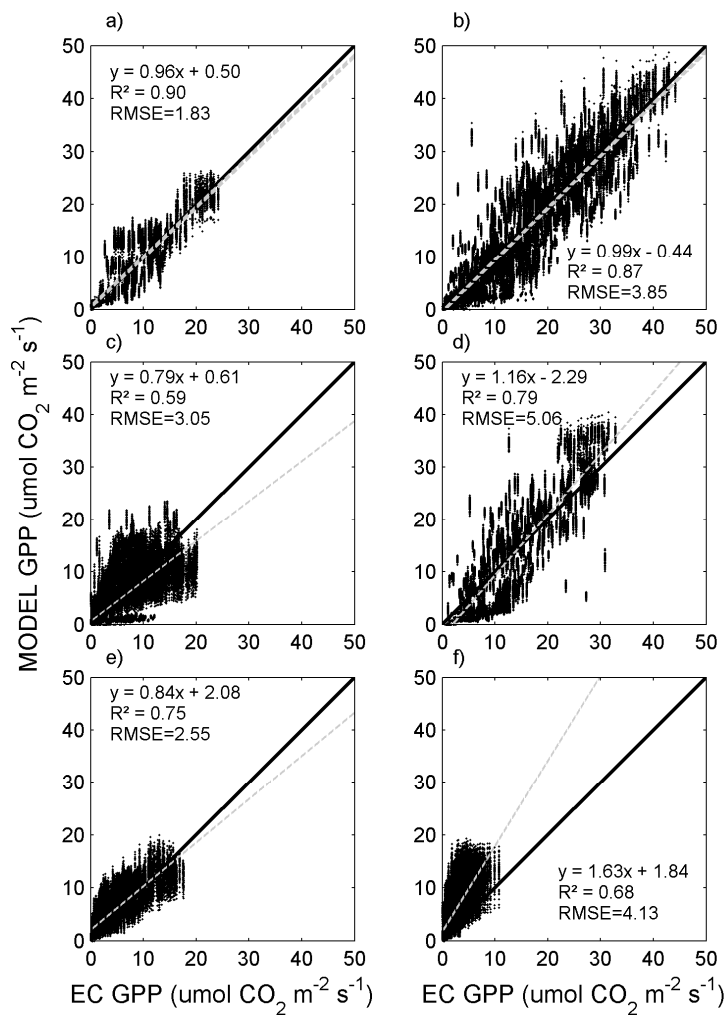
Figure 7. Evaluation of the modelled gross primary productivity (GPP) (Eq. 18) against in situ GPP for the six sites across Sahel (Figure 1). The thick black line shows the one-to-one ratio, whereas the dotted thin grey line is the fitted ordinary least square linear regression. The sites are a) Agoufou (ML-AgG), b) Dahra (SN-Dah), c) Demokeya (SD-Dem), d) Kelma (ML-Kem), e) Wankama Fallow (NE-WaF), and f) Wankama Millet (NE-WaM).